Journal of Innovative Optical Health Sciences
Vol. 2, No. 4 (2009) 365–374

World Scientific
www.worldscientific.com

FLUORESCENT IMAGES OF MITOCHONDRIAL REDOX STATES IN *IN SITU* MOUSE HYPOXIC ISCHEMIC INTESTINES

MAHSA RANJI[*,¶], SHOKO NIOKA[‡,‖], HE N. XU[§], BAOHUA WU[‡,§], LIN Z. LI[§], DWIGHT L. JAGGARD[†] and BRITTON CHANCE[‡]

[*]*Biophotonics Laboratory*
Department of Electrical Engineering and Computer Science
University of Wisconsin-Milwaukee, Milwaukee, WI 53211, USA

[†]*Department of Electrical and Systems Engineering*
University of Pennsylvania, Philadelphia, PA 19104, USA

[‡]*Department of Biochemistry and Biophysics*
University of Pennsylvania, Philadelphia, PA 19104, USA

[§]*Department of Radiology*
University of Pennsylvania, Philadelphia, PA 19104, USA

[¶]*ranji@uwm.edu*
[‖]*nioka@mail.med.upenn.edu*

We have imaged mitochondrial oxidation–reduction states by taking a ratio of mitochondrial fluorophores: NADH (reduced nicotinamide adenine dinucleotide) to Fp (oxidized flavoprotein). Although NADH has been investigated for tissue metabolic state in cancer and in oxygen deprived tissues, it alone is not an adequate measure of mitochondrial metabolic state since the NADH signal is altered by dependence on the number of mitochondria and by blood absorption. The redox ratio, NADH/(Fp + NADH), gives a more accurate measure of steady-state tissue metabolism since it is less dependent on mitochondrial number and it compensates effectively for hemodynamic changes. This ratio provides important diagnostic information in living tissues. In this study, the emitted fluorescence of mouse colon *in situ* is passed through an emission filter wheel and imaged on a CCD camera. Redox ratio images of the healthy and hypoxic mouse intestines clearly showed significant differences. Furthermore, the corrected redox ratio indicated an increase from an average value of 0.51 ± 0.10 in the healthy state to 0.92 ± 0.03 in dead tissue due to severe ischemia ($N = 5$). We show that the CCD imaging system is capable of displaying the metabolic differences in normal and ischemic tissues as well as quantifying the redox ratio *in vivo* as a marker of these changes.

Keywords: Optical diagnosis; NADH; flavoprotein; *in vivo*; ischemia; fluorescence.

1. Introduction

Previously, autofluorescence spectroscopies and imaging of NADH[1] and FAD have been used as an optical diagnostic tool for cancers,[2,3] ischemic diseases,[4,5] apoptosis,[6] and brain function.[7–11] Assessment of hypoxia would provide knowledge of oxygen delivery to mitochondria, the main tissue energy providers. Energy production in mitochondria is based upon the electron transport from fluorophores like NADH, FADH2 to O_2 in the respiratory chain by reduction and oxidation. The NADH autofluorescence is in the blue region (450 nm) upon UV excitation (366 nm). On the other hand, oxidized flavoprotein (Fp) including the

oxidized form of flavin adenine dinucleotide (FAD) emits at 520 nm when excited at 436 nm. Chance and Williams have investigated the metabolic states of NADH and other electron carriers[12–16] in detail and have shown that taking the ratio of NADH to Fp fluorescence provides a measure of steady-state metabolism in heart and brain.[17] We have previously employed the redox ratio to monitor cellular metabolism in a cryo-imaging set up.[6,8,18–20] Other researchers also investigated the concept of redox ratio *in vivo*[21,22] spectroscopically, and obtained redox images in animal models.[23]

The main challenge of *in vivo* studies of tissue metabolic state is the effects of hemoglobin absorption on excitation and fluorescence emission that induces dependence of fluorescence intensities on capillary densities. Also the fluorescence intensity of NADH and Fp are dependent on the density of mitochondria. Thus, we sought a redox state indicator using two fluorophores, NADH and Fp, rather than only NADH fluorescence intensity. Taking a ratio of the autofluorescence of NADH to Fp provides a more sensitive indicator of metabolic states independent of the number of mitochondria, and compensates for the artifact of blood absorbance. Most importantly, the changes in the NADH/(Fp + NADH) ratio stoichiometrically reflected the redox state changes. Redox state implies mitochondrial inner membrane potential that is related to ATP (energy) synthesis and cellular metabolism. It is also related to perturbations of substrate limitation and oxygen deprivation. A redox state indicator using the NADH and Fp redox ratio can provide key information on tissue metabolism.

This investigation applies the concept of the redox state measurement with a CCD camera to monitor *in vivo/in situ* tissue metabolism. We have implemented redox ratio imaging in hypoxic intestines as well as calibration procedures to quantify NADH and Fp fluorescence. The aim of this study is to use the redox ratio to assess the tissue oxidation–reduction state, to semi-quantitate this state and to characterize the normal and ischemic values of redox states.

2. Material and Method

2.1. *Subjects*

Five 100-gram adult mice were anesthetized with 5 mg/kg intraperitoneal injections of ketamine. The abdominal wall was excised to expose colons in the abdominal cavity. Then animals were placed on the optical stage beneath the CCD redox scanner camera. The control images of colon in live animals were first captured before pentobarbital sodium (50 mg/kg of body weight) was administered via the abdominal space to sacrifice the animal. When the pentobarbital was injected, redox scans were taken to detect the hypoxic ischemic effects until a few minutes after cessation of heart beat.

2.2. *Experimental set up*

The CCD optical set up is displayed in Fig. 1. The light from a broadband mercury arc lamp was incident on a cold mirror to exclude NIR wavelengths (heat). The rest of the light was spectrally filtered by optical bandpass filters to provide suitable excitation (EX) wavelengths. The filtered light was then obliquely incident on the tissue to minimize specular reflections and to excite fluorophores at different wavelengths. The induced emitted fluorescence from tissue was also spectrally filtered through a filter wheel to select

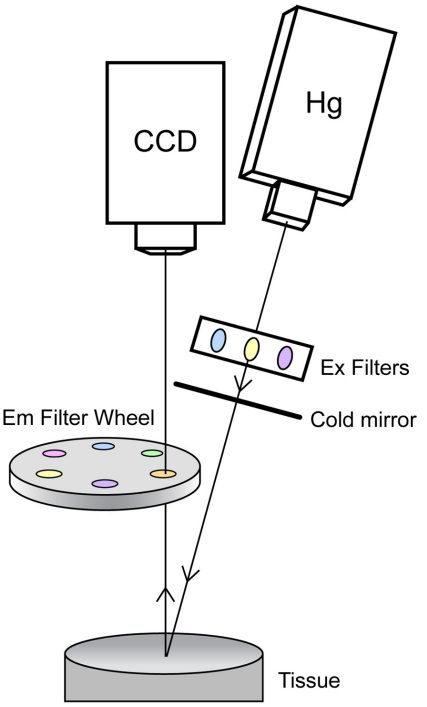

Fig. 1. The CCD optical imaging set up. Mercury light source passes through excitation filters and is incident on a cold mirror to exclude near infrared wavelengths (heat). The filtered light is then obliquely incident on tissue. The induced emitted fluorescence from tissue passes through emission filter wheel and was imaged on the CCD camera. CCD and Hg stand for charged coupled device and mercury, respectively.

emissions (EM) at suitable bandwidth for NADH and Fp. The wheel consisted of bandpass filters for NADH and Fp excitation (interference filters: 365HT25, 440DF20, Omega Optical, Brattleboro, VT, USA) and emission (interference filters: 455DF40, 525DF50, Omega Optical, Brattleboro, VT, USA). After passing through EM bandpass filters the light was then imaged on the CCD camera mounted over the filter wheel. The subjects were located on the sample stage, the height of which was adjustable for the best focus. At first the control images were captured and then after the pentobarbital injection, redox images were captured to monitor ischemia resulting from suppression of breathing. The acquisitions were averaged over 30 seconds to obtain a good S/N ratio. Finally, the fluorescent signals of dead tissue were acquired; they were apparently different than those of living animals.

2.3. *Calibration of NADH and Fp signal*

The purpose of the calibration was to establish the concentration dependence of Fp and NADH intensities. We quantified the effects of molarities on the fluorescence intensities and demonstrated the linearity of the CCD imaging signal response. For this purpose we used concentrations of 0, 70, 140, 280 μM of NADH (Disodium nicotinamide adenine dinucleotide, SIGMA Aldrich, St. Louis, MO) and 0, 24, 60, 120 μM of Fp (Flavin adenine dinucleotide disodium, SIGMA Aldrich, St. Louis, MO) standards. The desired amount of powder of each was weighed out and dissolved in 10 mM Tris-HCl buffer (pH = 7.5). These concentrations are comparable to physiological values.[24]

2.4. *Data acquisition and analysis*

A CCD camera (Cohu, San Diego, CA, model 2200, 8-bit digital output with resolution of 768 × 576, $10 \times 10\,\mu m^2$ pixels) captured the images and the software written in the lab produced BMP image format. The speed was 30 frames/s and 256 frames were averaged in real time. Prior to each image acquisition a reference frame was acquired by completely closing the lens to account for dark current. These reference frames were automatically subtracted from the EM images by the software. Later it was analyzed by a MATLAB code to account for absorption correction to get absolute fluorescence images. As previously explained, the incident light at NADH and Fp excitation wavelengths was bandpass filtered from a mercury arc lamp, and was incident on a stage with an angle of about 75° where the mouse tissue was located. The light intensity delivered to tissue was approximately $5\,\mu w/mm^2$ that was within the safe range for tissue. The emitted light was collected vertically through a filter wheel and imaged on the CCD. To account for the tissue absorption at UV and blue excitation wavelengths, the emission filters were set at the wavelengths of excitation to obtain absorption images $[\Psi_{\mathrm{NADH}}(ex); \Psi_{\mathrm{Fp}}(ex)]$. This absorption was later divided to the emitted fluorescence to correct for background signals and movement artifacts. The acquired data had an auto-adjusted intensity scale; thus, the first step was to convert it to the absolute light intensities. This absolute value was the difference of maximum and minimum of intensity counts divided by a normalization number (255). Fluorescence images $[\Psi_{\mathrm{NADH}}(em); \Psi_{\mathrm{Fp}}(em)]$ were acquired at the proper emission filters for NADH and Fp respectively. To correct for absorption at excitation, the absolute fluorescence intensities $[\Psi_{\mathrm{NADH}}(em); \Psi_{\mathrm{Fp}}(em)]$ were divided by absorption intensities as shown in Eqs. (1)–(3).

$$\Psi_{\mathrm{NADH}}(\mathrm{corrected}) = \Psi_{\mathrm{NADH}}(em)/\Psi_{\mathrm{NADH}}(ex), \quad (1)$$

$$\Psi_{\mathrm{FP}}(\mathrm{corrected}) = \Psi_{\mathrm{Fp}}(em)/\Psi_{\mathrm{Fp}}(ex), \quad (2)$$

$$\Psi_{\mathrm{Redox}}(\mathrm{corrected}) = \Psi_{\mathrm{NADH}}(\mathrm{corrected})/[\Psi_{\mathrm{Fp}}(\mathrm{corrected}) + \Psi_{\mathrm{NADH}}(\mathrm{corrected})]. \quad (3)$$

The redox ratio measures tissue oxygenation independent of mitochondrial density, fluorescence quenching, tissue absorption, as well as movement artifacts.

3. Results

3.1. *Calibration of NADH and Fp signal*

Figures 2(a) and 2(b) show the pseudo-colored fluorescence intensities of Fp and NADH for four different concentrations. To establish the instrument function of the CCD and test the linear response range, we fitted a straight line to the mean value of the intensities as indicated in Fig. 2(c). The correlation power is 0.98 for both Fp and NADH calibration curves. With these results, we showed not only the system linearity but also calibrated the

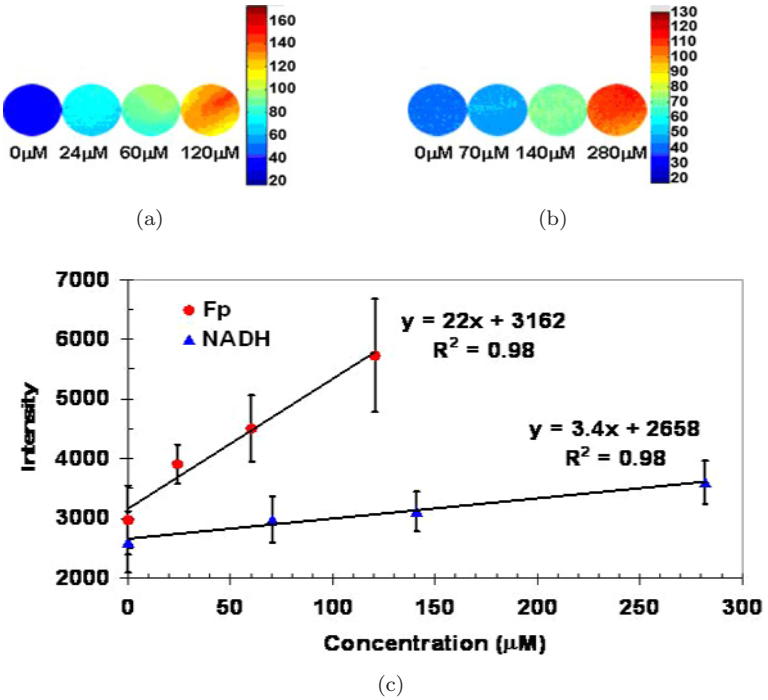

Fig. 2. (a) Fp and (b) NADH standard fluorescence intensities of different concentrations to demonstrate a linear correlation of intensity versus concentration. (c) Linearity of intensity versus concentration with a high correlation power for NADH and Fp solutions.

fluorescence intensity levels for these concentration ranges. The upper limits of the Fp and NADH linear response were 120 μM and 280 μM, respectively and we observed saturation when higher concentrations were used.

3.2. *In vivo/in situ fluorescence images*

Typical unprocessed images of NADH and FAD are shown in Fig. 3. NADH fluorescence intensity increases as the Fp signal decreases. These dramatic changes are mainly due to tissue hypoxia/ischemia and inhibition of complex I by pentobarbital resulting in an extremely high reduction of mitochondrial redox states. Lack of oxygen after death causes NADH and Fp to accumulate in reduced form and they are unable to transfer the electrons to oxygen in the electron transport chain.

These gray-scale pictures taken by CCD camera can be further processed to pseudo-color images for better clarity as explained in data analysis section. We processed these images to obtain absolute signals in control (live) and hypoxic (death) situations and to observe fluorescence intensity changes.

Figure 4 indicates the absolute data calculated by dividing the difference of the maximum and minimum of recorded image intensity by normalization factor (255). The first column displays Fp, the second column is NADH and the third shows the NADH redox ratio in live (top row) and dead animals (bottom row). As can be seen the NADH redox ratio at death is much higher due to ischemia and reduction of the fluorophores. A single Fp or NADH picture cannot give an accurate interpretation of tissue metabolic stage, but the redox ratio shows the difference clearly as illustrated in Figs. 4 and 5. The intensity bars do not have the same range since the intensity differences in Fp and NADH are large. However a quick examination shows that while the intensity of Fp decreased from an average of about 3000 to 2000, NADH signal increase was from 700 to 4000, which is disproportionally higher.

As previously explained, in order to correct for absorption at excitation wavelengths, the absolute fluorescence data were divided by absorption at excitation wavelengths to provide corrected signals as displayed in Fig. 5. To identify the differences in the mean of the redox ratio in the control and hypoxic tissues, the histograms of the intensity distributions were calculated (Fig. 6). The mean image intensities in this mouse show that the redox ratio increases from 0.59 in healthy tissue

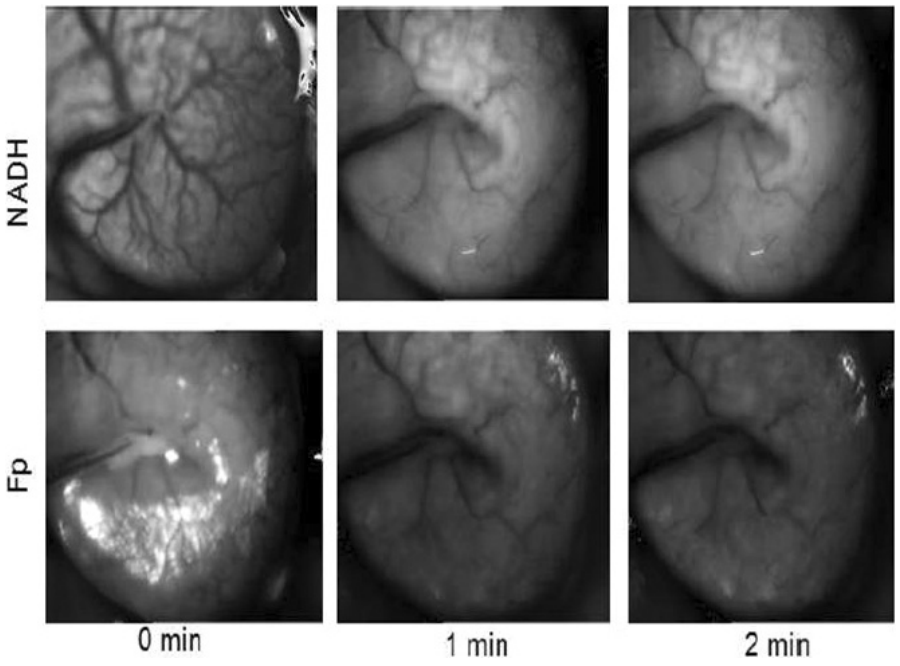

Fig. 3. Unprocessed fluorescence images of mouse colon; first column is control (live), second and third columns are one and two minutes after death, respectively. The top row is NADH images and the bottom row illustrates Fp images.

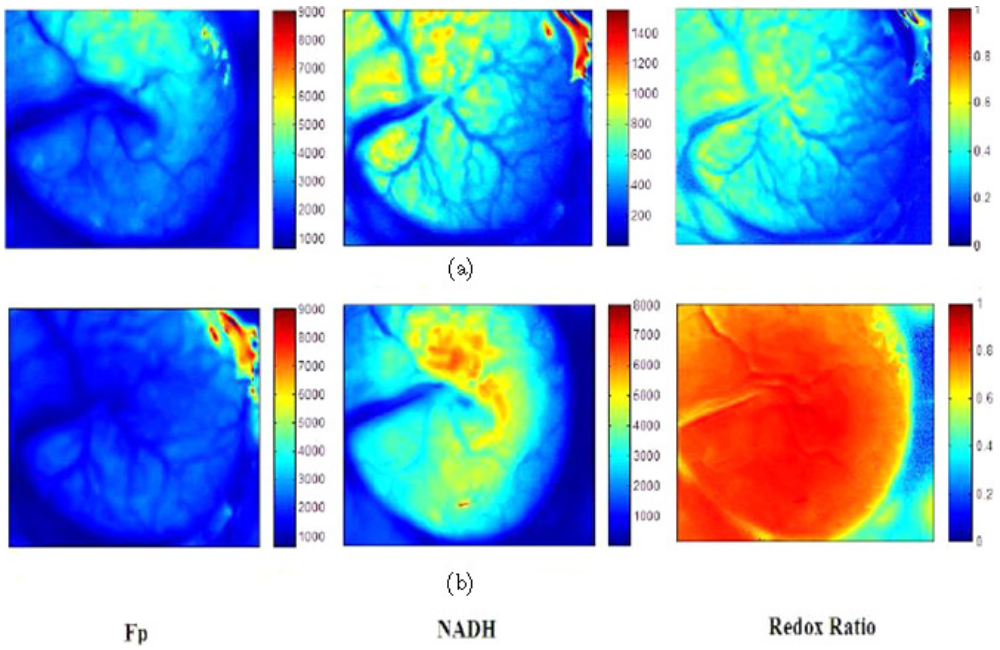

Fig. 4. (a) Absolute fluorescence (uncorrected) of live mouse colon. (b) Fluorescence (uncorrected) of dead mouse colon. First and second columns are Fp and NADH fluorescence intensities, respectively, and third column is NADH redox ratio.

to 0.95 in hypoxic tissue. This increase is due to tissue hypoxia/ischemia (State 5) and presumably also due to an inhibition of complex I by barbiturates leading to crossover phenomena (NADH reduction).[25,36] The results of five mice showed that the average redox ratio is 0.51 ± 0.10 (SD) for control and 0.92 ± 0.03 (SD) for two minutes after cessation of heart beat.

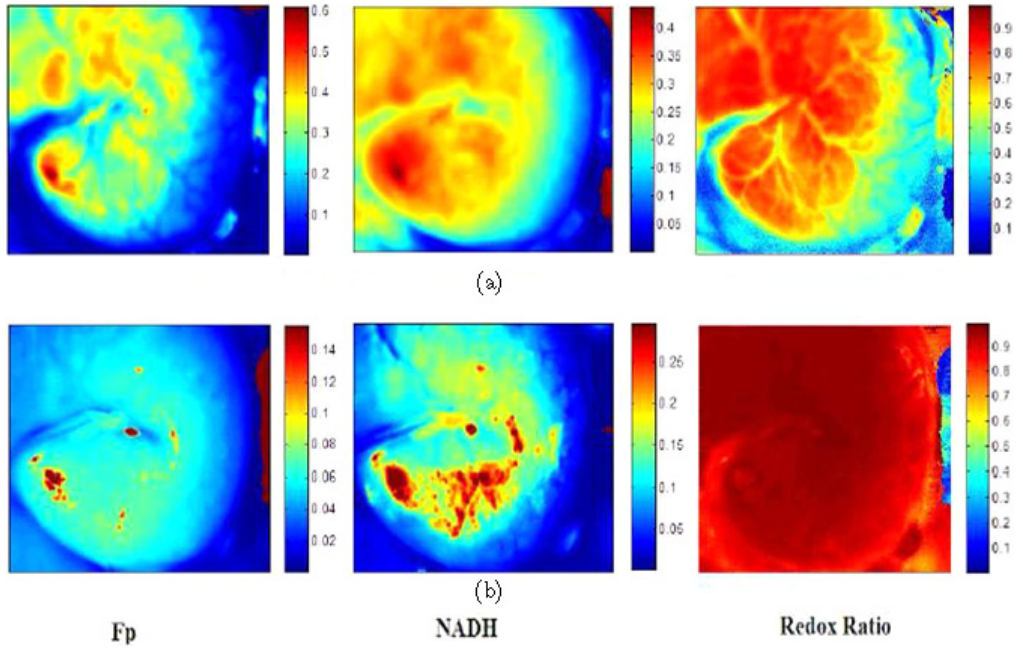

Fig. 5. (a) Corrected data of live mouse colon. (b) Corrected data of dead mouse colon. First and second columns are Fp and NADH data (%), respectively, third column is NADH redox ratio. The redox ratio after death is very high (red color) due to severe hypoxia/ischemia and inhibition by pentobarbital.

4. Discussion

Mitochondrial oxidative phosphorylation is the process by which ATP is produced as electrons are transferred from NADH and FADH2 to O_2 via the electron transport chain of enzymes. NADH and FADH2 are energy-rich molecules and the storage of energy is influenced by many conditions and reflects redox states or transmembrane electrical potential.

Chance *et al.* defined redox states in isolated mitochondria *in vitro*.[12–16] The mitochondrial stage in which ATP is actively synthesized is called State 3, the states of oxygen and substrate deprivation are State 5 and State 2 respectively, the resting state without ADP is called State 4, and the state with limited endogenous substrate and low ADP is called State 1. The NADH redox state oxidizes from resting (State 4) to highly active state (State 3). Thus, NADH redox state is an indicator of monitoring cellular metabolic activity through mitochondrial oxidative phosphorylation. State 5 is the most frequent clinically-encountered state in which the concentration of chemically reduced form of NADH rises when ATP production is not sufficient to meet cellular demand due to lack of oxygen. In the living cells, physiological mitochondrial states are usually in between State 3 and State 4, where the NAD^+/NADH ratio is closely correlated with the rate of ATP production.

Chance's group demonstrated that the fluorescence signal from heart tissue originates mostly from NADH in the mitochondria and the contribution of NADPH — present in cytosol — is very small.[26,27] To further investigate this, they also compared the fluorescence of NADH and NADPH of liver *in vivo*.[28] They showed that NADH signal increased during induction of ischemia, while NADPH signal did not change. Other researchers also showed that the origin of NADH fluorescence is from the bound NADH in mitochondria.[29,30] The quantum yield of NADH when it is bound to proteins is approximately four folds higher.[31]

Another electron carrier in ATP production, besides NADH, is electron transfer flavoprotein-ubiquinone-oxidoreductase (ETF-QO) that is bound to the inner mitochondrial membrane. It accepts electrons from electron transfer flavoprotein (ETF) located in the mitochondrial matrix, and transfers them to ubiquinone in the inner mitochondrial membrane, thus linking the primary flavoprotein dehydrogenases with ubiquinol-cytochrome c reductase (cytochrome bc1 complex

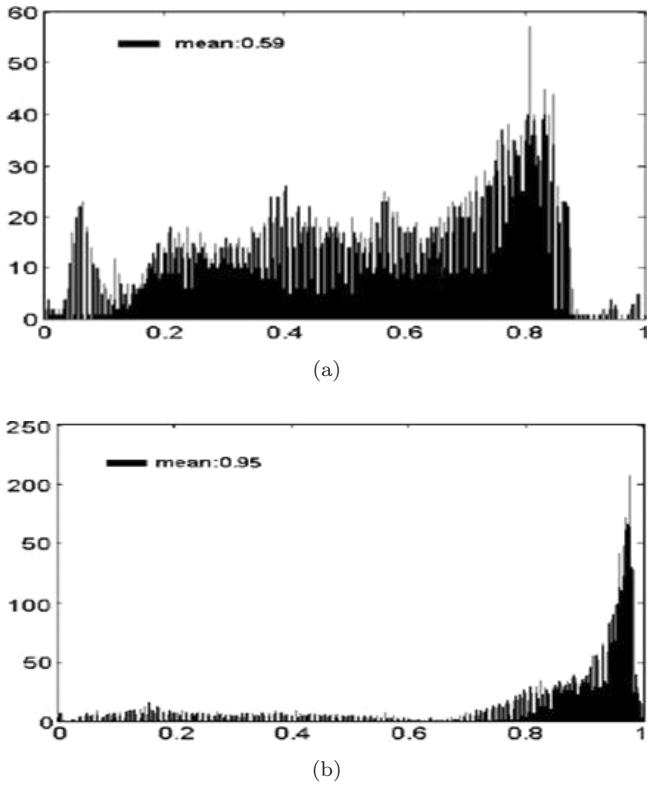

Fig. 6. (a) Histogram of corrected redox ratio of a live mouse colon. (b) Histogram of corrected redox ratio of a dead mouse colon. The red shift in the mean value of redox ratio in the dead mouse colon is due to severe hypoxia/ischemia and inhibition by pentobarbital.

or complex III). ETF-QO, together with ETF, is an essential component of fatty acid metabolism and the catabolism of some amino acids.

In a clinical situation, e.g., oxygen-deprived tissue such as ischemia/hypoxia (State 5), a high NADH state has been detected in the heart[32,33] and brain,[33] kidney[34] and brain stroke model.[8] Functional imaging studies of brain demonstrate that neuronal activity induces a lower redox state (State 3) by FAD fluorescence.[9–11] Furthermore, high NADH has been detected in freeze-trapped cancer tissue,[19,20] as well as in human cervical cancer tissue.[1] However, recently we found that more aggressive melanoma mouse xenografts have a signature of lower redox states, i.e., oxidation of NADH, and a higher Fp redox ratio, i.e., Fp/(Fp + NADH).[35] In our model, the NADH redox ratio exhibited significant increase in dead tissue vs control. Figure 5 shows a redox ratio of 0.92 that is almost as high as we can get. Other research suggests that ischemia and hypoxia took at least three minutes to achieve the highest redox state.[24] This very high redox state is probably achieved by not only hypoxia/ischemia of State 5, but also the effects of pentobarbital that inhibits complex I,[36] leading to high NADH reduction.[25,36,37]

CCD imaging is a purely noninvasive/nontissue destructive technique that does not need any tissue contact. Our data indicated that this technique can be useful in assessing *in vivo* and *in situ* tissue oxygenation in small animal studies. Mitochondrial redox signals are indeed indicators of tissue hypoxia[38] that can be captured by fluorescence imaging. In the hypoxic phase, the autofluorescence signals increase in agreement with the accumulation of reducing equivalents as a consequence of the complete oxygen depletion. We have used reflectance signals from colon tissue to correct the fluorescence signals of NADH and Fp for incident light normalization, while incident light can fluctuate mostly due to hemodynamic artifacts. Corrected NADH and Fp signals quantitate better the tissue oxidation–reduction state compared to that attempted by others.[3]

We have attempted to quantify NADH and FAD by calibration studies shown in Fig. 2. However in this paper, we have only achieved partially. Using solution standards, we were able to obtain the linear dynamic range of the CCD redox imager and the ratio between channel Fp and channel NADH. These ratios are highly influenced by light source, both the excitation and emission filters and detector efficiency as well as background signals of tissues or solutions. Thus the ratios will change in each device and each sample. As a result, the nominal concentration of Fp and NADH in the colon tissue can only be estimated very roughly as anywhere between 0 to 120 μM and 0 to 280 μM respectively. We did not determine the nominal concentration of NADH and Fp for the tissue at this time since the images of solution standards were not acquired at the same time of the biological sample and the running conditions of instruments could also be different. In another paper, we have determined the nominal concentration of these fluorophores in tissue by imaging the tissue sample and the solution standards together in cryosamples.[39,40] We have not found any report on the actual concentration of these fluorophores in colon tissue. Only few references are available in other tissues, for example, about 300 μM of NADH in Liver.[26]

It is important to note that the excitation and emission wavelengths of NADH and Fp are completely separated, hence providing highly specific and sensitive signals compared to absorption

spectroscopic signals. Another concern of tissue fluorometry is that tissues have some specific absorbers and fluorophores that may alter, influence and interact with one another, thus creating some inaccuracy for our redox state imaging based on the NADH and FAD measurements. Specifically, hemoglobin, red blood cells and water contents changed dramatically in our model. Hemoglobins have very high absorptions in Soret band of 400–450 nm, their concentrations in the living tissue are of an order of 100 μM, and any changes in the blood flow will change the hemoglobin concentration (in the case of ischemia, decrease in red blood cells is expected). Similarly, hypoxia (decrease in HbO_2 and increase in Hb) which occurred before NADH reduction[3] will also change absorption sensitivity in those excitation and emission light intensities at different wavelengths.

Mayevsky and Rogatsky have shown that taking the reflectance (light intensity at excitation wavelength) as a reference from emission light can compensate quite reasonably for the real NADH fluorescence intensity.[3] That is also the basis for our correction in this paper as shown in Eqs. (1)–(3). In our model, the absolute NADH fluorescence intensity increases from 800 to 4,000 (five times) due to the decrease in background absorption by hemoglobin Soret band as well as increase in NADH (Fig. 4). On the other hand, when it is corrected by the excitation light intensity (incident light), the actual NADH fluorescence intensity contribution was decreased from 0.25% to less than 0.2%. Moreover, the decrease in Fp signal is much more than that of NADH, which made effective redox ratio very high as 0.92 (Fig. 5). This relative fluorescence intensity decrease cannot be explained by the absorption of blood, whose volume decrease can only increase the light intensity. We might consider photobleaching, an increase in tissue scattering as well as moving artifact by total tissue volume decrease which can decrease the light intensity. Photobleaching is a common problem for any experiment. In particular, exposure time of a few minutes to photons is large enough during and after pentobarbital injection, even though the intensity of each excitation light is of an order of microwatt per mm^2.

In short, an optical, non-tissue destructive imaging device allows the quantitative regional assessment of tissue oxidation states at the cellular level *in vivo*. Such a technique may allow measurements of the degree of hypoxia in disease diagnosis. Alteration in tissue oxygen supply directly influences autofluorescence properties, and time-course images of the emission signal provide tissue diagnostic parameters. By applying this method, normal and hypoxic mouse intestines showed normal and reduced form of mitochondrial fluorescence images. Quantitation of fluorescence emission and redox imaging are essential for *in vivo* diagnosis to identify normal and hypoxic tissue states. The mean redox ratio increase of 56% in the ischemic tissue is a simple though powerful method to evaluate cell metabolic status. These animal-study results open a door to clinical transferability of metabolic monitoring by fluorescence imaging in different surgeries.

Acknowledgments

This work was supported in part by the NIH grant R44 CA-96016, an NIH supported research resource P41-RR02305 and the Network of Translational Research in Optical Imaging (NTROI) at the University of Pennsylvania (U54 CA105008) and a Career Catalyst Award from Susan G. Komen Foundation (KG081069).

References

1. R. Drezek, K. Sokolov, U. Utzinger, I. Boiko, A. Malpica, M. Follen, R. Richards-Kortum, "Understanding the contributions of NADH and collagen to cervical tissue fluorescence spectra: Modeling, measurements, and implications," *J. Biomed. Opt.* **6**, 385–396 (2001).
2. T. D. Wang, J. M. Crawford, M. S. Feld, Y. Wang, I. Itzkan, J. Van Dam, "*In vivo* identification of colonic dysplasia using fluorescence endoscopic imaging," *Gastrointest. Endosc.* **49**, 447–455 (1999).
3. A. Mayevsky and G. Rogatsky, "Mitochondrial function *in vivo* evaluated by NADH fluorescence: From animal models to human studies," *Am. J. Physiol. Cell. Physiol.* **292**, C615–C640 (2007).
4. M. Tamura, N. Oshino, B. Chance, I. A. Silver, "Optical measurements of intracellular oxygen concentration of rat heart *in vitro*," *Biochem. Biophys.* **191**, 8–22 (1978).
5. O. G. Bjornsson, K. Kobayashi, J. R. Williamson, "Inducers of adenylate cyclase reverse the effect of leukotriene D4 in isolated working guinea pig heart," *Am. J. Physiol.* **252**, H1235–H1241 (1987).
6. M. Ranji, D. L. Jaggard, B. Chance, "Observation of mitochondrial morphology and biochemistry changes undergoing apoptosis by angularly resolved light scattering and cryoimaging," *Proc. SPIE* **6087**, 60780K1–60780K9 (2006).

7. S. Nioka, D. S. Smith, B. Chance, H. V. Subramanian, S. Butler, M. Katzenberg, "Oxidative phosphorylation system during steady-state hypoxia in the dog brain," *J. Appl. Physiol.* **68**, 2527–2535 (1990).
8. A. Shino, M. Haida, B. Beauvoit, B. Chance, "Three-dimensional redox image of the normal gerbil brain," *Neuroscience* **91**, 1581–1585 (1999).
9. M. Tohmi, K. Takahashi, Y. Kubota, R. Hishida, K. Shibuki. "Transcranial flavoprotein fluorescence imaging of mouse cortical activity and plasticity," *J. Neurochem.* **109**, 3–9 (2009).
10. B. L'Heureux, H. Gurden, F. Pain, "Autofluorescence imaging of NADH and flavoproteins in the rat brain: Insights from Monte Carlo simulations," *Opt. Express.* **17**, 9477–9490 (2009).
11. D. A. Llano, B. B. Theyel, A. K. Mallik, S. M. Sherman, N. P. Issa, "Rapid and sensitive mapping of long-range connections *in vitro* using flavoprotein autofluorescence imaging combined with laser photostimulation," *J. Neurophysiol.* **101**, 3325–3340 (2009).
12. B. Chance, G. R. Williams, "Respiratory enzymes in oxidative phosphorylation. I. Kinetics of oxygen utilization," *J. Biol. Chem.* **217**, 383–393 (1955).
13. B. Chance, G. R. Williams, "Respiratory enzymes in oxidative phosphorylation. II. Difference spectra," *J. Biol. Chem.* **217**(1), 395–407 (1955).
14. B. Chance, G. R. Williams, "Respiratory enzymes in oxidative phosphorylation. III. The steady state," *J. Biol. Chem.* **217**(1), 409–427 (1955).
15. B. Chance, G. R. Williams, "Respiratory enzymes in oxidative phosphorylation. IV. The respiratory chain," *J. Biol. Chem.* **217**(1), 429–438 (1955).
16. B. Chance, G. R. Williams, W. F. Holmes, J. Higgins, "Respiratory enzymes in oxidative phosphorylation. V. A mechanism for oxidative phosphorylation," *J. Biol. Chem.* **217**, 439–451 (1955).
17. B. Chance, B. Schoener, R. Oshino, F. Itshak, Y. Nakase, "Oxidation–reduction ratio studies of mitochondria in freeze-trapped samples," *J. Biol. Chem.* **254**, 4764–4771 (1979).
18. A. Shino, M. Matsuda, J. Handa, B. Chance, "Poor recovery of mitochondrial redox state in CA1 after transient forebrain ischemia in gerbils," *Stroke* **46**, 2421–2425 (1999).
19. N. Ramanujam, R. Richards-Kortum, S. Thomsen, A. Mahadevan-Jansen, M. Follen, B. Chance, "Low temperature fluorescence imaging of freeze-trapped human cervical tissues," *Optics Express* **8**, 335–343 (2000).
20. Z. Zhang, Q. Liu, Q. Luo, M. Zhang, D. Blessington, L. Zhou, L. A. Chodosh, G. Zheng, B. Chance, "3D imaging of the metabolic state of c-MYC-induced mammary tumor with the cryo-imager," *Proc. SPIE* (San Hose 2003) 647–655 (2003).
21. K. Tsubota, R. A. Laing, K. R. Kenyon, "Noninvasive measurements of pyridine nucleotide and flavoprotein in the lens," *Invest. Ophthalmol. Vis. Sci.* **28**, 785–789 (1987).
22. B. M. Paddle, G. Brown, P. Vincent, "Scanning fluorometer for the rapid assessment of pyridine nucleotide and flavoprotein fluorescence changes in tissues *in vivo*." *J. Biomed. Eng.* **8**, 334–340 (1986).
23. B. J. Wong, V. Wallace, M. Coleno, H. P. Benton, B. J. Tromberg, "Two-photon excitation laser scanning microscopy of human, porcine, and rabbit nasal septal cartilage," *Tissue Eng.* **7**, 599–606 (2001).
24. A. Ghosh, D. Finegold, W. White, K. Zawalich, F. M. Matschinsky, "Quantitative histochemical resolution of the oxidation–reduction and phosphate potentials within the simple hepatic acinus," *J. Biol. Chem.* **257**, 5476–5481 (1982).
25. B. Chance, G. Hollunger, "Inhibition of electron and energy transfer in mitochondria, 1. Effects of amytal, thiopental, rotenone, progesterone and methylene glycol," *J. Biol. Chem.* **238**, 8–31 (1963).
26. B. Chance, H. Baltschefsky, "Respiratory enzymes in oxidative phosphorylation. VII. Binding of intramitochondrial reduced pyridine nucleotide," *J. Biol. Chem.* **233**, 736–739 (1958).
27. B. Chance, P. Cohen, F. Jobsis, B. Schoener, "Intracellular oxidation–reduction states *in vivo*," *Science* **137**, 499–508 (1962).
28. B. Chance, D. Jamieson, J. R. Williamson, "Control of the oxidation–reduction state of reduced pyridine nucleotides *in vivo* and *in vitro* by hyperbaric oxygen," *Third International Conference on Hyperbaric Medicine, National Academy of Sciences*, p. 1541 (1966).
29. J. B. Chapman, "Fluorometric studies of oxidative metabolism in isolated papillary muscle of the rabbit," *J. Gen. Physiol.* **59**, 135154 (1972).
30. M. J. O'Connor, F. Welsh, L. Komarnicky, L. Davis, J. Stevens, D. Lewis, C. Herman, "Origin of labile NADH tissue fluorescence," *Oxygen Physiol. Function*, p. 9099 (1977).
31. J. R. Lakowicz, *Principles of Fluorescence Spectroscopy*, Plenum, New York (1985).
32. J. M. C. C. Coremans, C. Ince, H. A. Bruining, G. J. Puppels, "Semi-quantitative analysis of reduced nicotinamide adenine dinucleotide fluorescence images of blood-perfused rat heart," *Biophysical Journal* **72**, 1849–1860 (1997).
33. C. H. Barlow, W. R. Harden III, A. H. Harken, M. B. Simson, J. C. Haselgrove, B. Chance, M. O'Connor, G. Austin, "Fluorescence mapping of mitochondrial redox changes in heart and brain," *Crit. Care Med.* **7**, 402406 (1979).
34. R. S. Balaban, L. J. Mandel, "Metabolic substrate utilization by rabbit proximal tubule. An NADH

fluorescence study," *Am. J. Physiol. Renal Fluid Electrolyte Physiol.* **254**, F407F416 (1988).
35. L. Z. Li, R. Zhou, H. N. Xu, L. Moon, T. Zhong, E. J. Kim, H. Qiao, D. Leeper, B. Chance, J. D. Glickson, "Quantitative magnetic resonance and optical imaging biomarkers of melanoma metastatic potential," *Proc. Natl. Acad. Sci. USA* **106**, 6608–6613 (2009).
36. J. P. Weiss, C. H. Barlow, B. Chance, "Pentobarbital-induced reduction of pyridine nucleotide measured by surface fluorometry in perfused rat heart," *Biochem. Pharmacol.* **15**(27), 1510–1511 (1978).
37. M. Gutman, T. P. Singer, H. Beinert, J. E. Casida, "Reaction sites of rotenone, piericidin A, and amytal in relation to the nonheme iron components of NADH dehydrogenase," *Proc. Natl. Acad. Sci. USA* **65**, 763–770 (1970).
38. S. Nioka, K. McCully, G. McClellan, J. Park, B. Chance, "Oxygen transport and intracellular bioenergetics on stimulated cat skeletal muscle," *Adv. Exp. Med. Biol.* **510**, 267–272 (2003).
39. H. N. Xu, B. Wu, S. Nioka, B. Chance, L. Z. Li, "Calibration of CCD-based redox imaging for biological tissues," in Medical Imaging 2009: Biomedical Applications in *Molecular, Structure, and Functional Imaging*, *Proceedings of SPIE*, **7262**, 72622F1–7 (2009).
40. H. N. Xu, B. Wu, S. Nioka, B. Chance, L. Z. Li, "Quantitative redox scanning of tissue samples using a calibration procedure," *J. Innov. Opt. Health. Sci.* **2**(4), 375–385 (2009).